JOURNAL OF AIRCRAFT
Vol. 43, No. 2, March–April 2006

Buckling Analysis and Minimum-Mass Design Procedures for Composite Wing-Box Structures

C. B. York*
University of Glasgow, Scotland, United Kingdom

This study investigates the minimum-mass design of composite wing-box structures employing a syntactic film core (SynCore™) as a partial replacement for carbon-fiber material. Special attention is given to the balance between buckling strength and the limiting strain constraints of the two materials. Symmetric and antisymmetric angle-ply stacking sequences, with specially orthotropic properties, are combined to form the special orthotropic laminate skin of the wing box. Computer modeling accounts for continuity of the skin over composite curved root-channel-section spars, which are assumed to be connected by a single line of closely spaced bolts. Emphasis is also placed on the level of sophistication of the modeling and the level to which modeling approximations may be safely applied. The effects of analyzing a panel with its true skewed shape, rather than approximating it as rectangular in plan, are compared with the infinitely long panel representation on which the optimization study is based. Two design strategies are adopted in the study whereby either skin-ply thickness is the independent variable and the outer mold line of the wing box is maintained by linking the spar depth (dependant variable) or the spar pitch is the independent variable and all plies are held at their correct physical thicknesses.

Nomenclature

A_{ij}, B_{ij}, D_{ij}	=	extensional, bending, extensional-bending stiffness (i, $j = 1, 2, 6$)
a	=	plate/panel length
b	=	plate/panel width
M_{P0}, M_{Popt}	=	datum, optimized panel mass
M_{T0}, M_{Topt}	=	datum, optimized wing mass including fasteners
M_{W0}, M_{Wopt}	=	datum, optimized wing mass
N_x, N_y, N_{xy}	=	in-plane longitudinal, transverse, shear load/unit length
t, t_{opt}	=	ply thickness, optimized ply thickness
t_{skin}, t_{spar}, $t_{SynCore}$	=	skin, spar, SynCore thickness
α	=	skew angle
θ	=	principal compressive stress direction
λ	=	buckling half wavelength
σ, τ	=	in-plane compressive, shear stress

Subscripts

A	=	antisymmetric stacking sequence
S	=	symmetric stacking sequence
T	=	true stacking sequence

I. Introduction

A previous optimization study by the author and colleagues[1] considered the most heavily and lightly loaded of eight benchmark stiffened laminated wing panels defined from a Dornier wing by a GARTEUR (Group for Aeronautical Research and Technology in Europe) working party. These benchmark panels had three identical and equally spaced stiffeners. The results were chosen to help designers understand many important aspects of the choice of design variables and the effects of changing the sophistication of modeling and theory used for a wide range of wing panels. The principal design variables were skin and stiffener ply thicknesses and stiffener height, shape, and pitch. Additional factors were also considered, such as the effects of including the stiffening effect of adjacent spars, including the effects of continuity with laterally adjacent panels, including through thickness shear (TTS) deformation in the panel analysis, and analyzing the panel with its true skewed shape rather than approximating it as rectangular in plan.

Although the effect of the stiffener shape and pitch was the primary focus in the work described, the current study considers a multispar wing-box configuration with unstiffened skin. The primary focus of attention is now the composition of the composite laminate skins, together with the influence of material-strain constraints, which were found to be inactive in the previous optimization study for stiffened panels. Furthermore, the combined effects of supporting spars and of continuity with adjacent panels are present in all the panel variants considered, rather than as a single panel variant.

The present study arises from related work performed by the author while on a recent secondment to BAE Systems. The paper describes a weight-trade study for preliminary design of composite empennage structures based on optimized panel-level designs. The loading and general orthotropic material properties for the start design were obtained from a finite-element analysis of the entire aircraft and therefore represent a single iteration within a multilevel optimization procedure. The new results presented here should help engineers draw useful conclusions without requiring access to any restricted BAE Systems material. However, the relationship to the BAE Systems work has ensured that the results presented are for a practical problem that is likely to be applicable to other empennage structures.

One of the main design strategies generally adopted by industry is to size structural components using simplified analysis assumptions, which generally give lower-bound buckling solutions. They therefore give conservative (upper-bound) solutions in design. This is of course appropriate for conservative structural design and initial sizing, but where the structure is weight critical it is important to explore more sophisticated analysis methods, probing for further reductions in weight without compromising structural integrity.

The objective of the current study is therefore to assess the structural-weight implications of changing the level of sophistication of modeling and theory used, and demonstrate these implications through the buckling analysis and sizing of composite skins and spars relating to a number of empennage structures with similar wing-box configurations.

From these initial investigations, more specific studies of panel stability are then pursued, concerning the ply-stacking-sequence

Received 24 February 2005; revision received 27 May 2005; accepted for publication 9 June 2005.

*Senior Lecturer, Department of Aerospace Engineering.

definition, otherwise characterized by the percentage of plies in each of the preferred orientations, TTS effects, the introduction of low-density Syntactic film core as a partial replacement for carbon-fiber material, and ultimately a multispar weight-trade study.

II. Preliminary Buckling-Analysis Study

A. Details of the Modeling and Theory Used

The eigenvalue buckling-analysis (and optimum-design) study was performed on the assumption that the panels were infinitely long, because this is frequently done in practice and was the standard adopted for preliminary sizing studies at BAE Systems. However, ribs and spars often divide the skin into smaller aspect-ratio quadrilaterals, which can be better approximated by parallelograms. Therefore, some preliminary analysis results are presented to show the difference in buckling strength made by the alternative assumptions of rectangular and parallelogram planform approximations and variation in boundary conditions, which include simple supports, spar supports, and clamped supports. All variants are compared against the infinitely long panel with simply supported edges, that is, the datum case used throughout the study.

Because of the nature of the theory used to obtain these results, the longitudinal edge supports are represented exactly but the transverse line supports (inclined to give a parallelogram planform) are instead represented by a sufficient number of point supports. Note that for high aspect-ratio panels, these transverse line supports have little effect on the initial buckling strength, which converges on the infinitely long panel results as the aspect ratio of the panel increases.

A more sophisticated variant, incorporating the rotational stiffness of realistic spar supports, included the effects of continuity of the panel skin. The spars themselves were unloaded, composite, curved-root channel sections, assumed to be connected to the skin by a single line of bolts and approximated by a rigid line connection. Symmetry conditions were also employed and therefore only the top half of the spar was modelled.

The panel-buckling analysis and optimum-design code VICONOPT[2,3] (VIPASA with constraints and optimization), used throughout the study, is based on the stiffness-matrix method with exact flat plate theory. The stiffness matrices derived for each plate may optionally allow for the effects of transverse shear deformation, with the assumption that the shear angle corresponding to rotations about the in-plane normal at a plate edge must be zero at junctions between plates.[4] Two types of analysis are used, which are based on those of the earlier programs VIPASA and VICON. The theory of VIPASA (vibration and instability of plate assemblies with shear and anisotropy) analysis assumes that the mode of buckling varies sinusoidally in the longitudinal direction with half wavelength λ. Nodal lines, or lines of zero buckling displacement, are straight and perpendicular to the longitudinal direction, that is, in the transverse direction, if all plates are orthotropic and no shear loading is present. Simply supported end conditions are satisfied in this case. Otherwise, solutions only approximate such end conditions and become excessively conservative as λ approaches the panel length a.

VICON (VIPASA with constraints) theory uses Lagrangian multipliers to impose the constraints representing point supports, so that for instance a shear loaded panel supported along rectangular boundaries can be accurately represented. To achieve this, the analysis couples stiffness matrices for different wavelengths, derived from the VIPASA theory, to enforce the required number and location of nodal points in the resulting mode shape. Thus, results are for an infinitely long plate assembly, with supports repeating at intervals a. Plate assemblies that repeat in the transverse direction are analyzed by using infinite-width recurrence relations so that analysis involves only a datum repeating portion.[5] Point supports can be introduced at any longitudinal position in the panel, and the combination of this capability with the transverse repetitive analysis permits a very efficient method for analysing skewed panels.[6]

Half wavelengths, which are coupled in the computer code VICONOPT, are defined by $\lambda = a/(\xi + 2q)$, where $q = 0, 1, \ldots, 10$ and $\xi = 0, 0.25, 0.5, 0.75$, and 1 were considered. Alternatively, where short wavelength (or local) buckling was identified in higher aspect-ratio panels, buckling calculations can be performed for (uncoupled) half wavelengths of $\lambda = a/i$ ($i = 1, 2, 3, \ldots, 10$) to reduce computation time, while still maintaining the accuracy achieved by coupling wavelengths.

The optimization technique combines the well-proven mathematical programming optimizer CONMIN,[7] which incorporates the method of feasible directions, and a method that scales the design to achieve and maintain feasibility.[3]

The design problem is a constrained-minimization problem in which the inequality constraints include buckling and material-strength requirements together with configuration constraints. The objective function is the mass of the plate assembly. In this study the plate breadths and layer thicknesses of the skin are design (i.e., independent) variables, whereas other plate breadths and layer thicknesses, for example, those of the spars, along with plate offsets, are either held fixed or are linked to the design variables to become dependent variables. The design strategy within VICONOPT involves the calculation of sensitivities for the buckling-load factors with respect to design variables. CONMIN then performs linear optimization to minimize the panel mass, subject to these sensitivities and the configuration constraints described previously.

B. Preliminary Analysis Results

Results from the preliminary analysis study allows the buckling strength of thin composite panel structures to be evaluated for combinations of uniform in-plane compression and shear loading. These results highlight the specific effects of realistic planform geometry, physical continuity with adjacent panel skins, and the additional restraint provided by torsionally stiff supporting spars. They are presented in the form of either nondimensional buckling interaction curves, or their derivatives, illustrating how these factors lead to improvements (percentage increase) in buckling strength above a datum configuration (Case 1—Inf) consisting of an infinitely long panel with simply supported edges.

Details of the geometry and material properties used for the preliminary analysis follow. The panel width $b = 300$ mm (11.8 in.), and length $a = 750$ mm (29.5 in.). The skew angle of the panel planform $\alpha = 33$ deg. The supporting spar flange width $= 38.1$ mm (1.5 in.), and overall depth $= 76.2$ mm (3 in.), with a root radius $= 2t_{\text{spar}}$ at the flange/web interface. The skin had a symmetric 20-ply specially orthotropic laminate $[45/90/-45_2/90/\pm 45/0_2/45]_S$ of total thickness $t_{\text{skin}} = 2.794$ mm (0.11 in.), and the spar had a symmetric 16-ply specially orthotropic laminate $[\pm 45/-45/45/90/-45/45/0]_S$ of total thickness $t_{\text{spar}} = 2.235$ mm (0.088 in.). The material used had the following properties: $E_{11} = 161.0$ GPa, $E_{22} = 11.38$ GPa, $\nu_{12} = 0.32$, and $G_{12} = 5.17$ GPa.

The buckling-interaction curves of Fig. 1 are used to demonstrate the procedure for generating the curves of buckling-strength increase in Fig. 2 for each of the boundary conditions illustrated in Fig. 3. All comparisons of buckling-strength increase are based on the case 1—Inf datum panel, that is, the infinitely long panel with simply supported edges. The combination of in-plane compression and shear loading (where 1 N/mm $\cong$ 5.7 lb/in) can be transformed into a principal compressive-stress direction. These principal compressive-stress directions (θ) are illustrated by the radial lines superimposed on Fig. 1, where positive and negative shear loading have principal compressive-stress direction of $\theta = 45$ deg and -45 deg, respectively. A pure compression load has a principal compressive-stress direction of $\theta = 0$ deg. Combined loading has values between these bounds. The example given is for the case of $\theta = -35$ deg. Figure 2 provides the buckling-strength comparisons for the complete range of load combinations shown in Fig. 1, calculated as the ratio of the buckling ordinate for case 4—Inf, and so forth, with respect to the ordinate for case 1—Inf, and expressed as a percentage. For clarity on Fig. 1, only the symmetric half of the each interaction curve is shown.

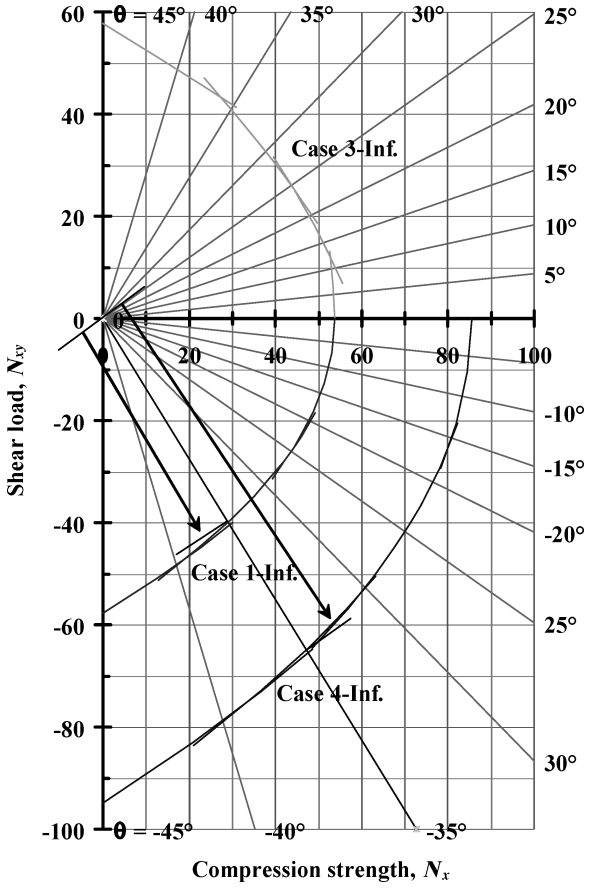

Fig. 1 Buckling-interaction diagram demonstrating the calculation of buckling-strength increase with respect to principal compressive-stress direction θ used in Fig. 2.

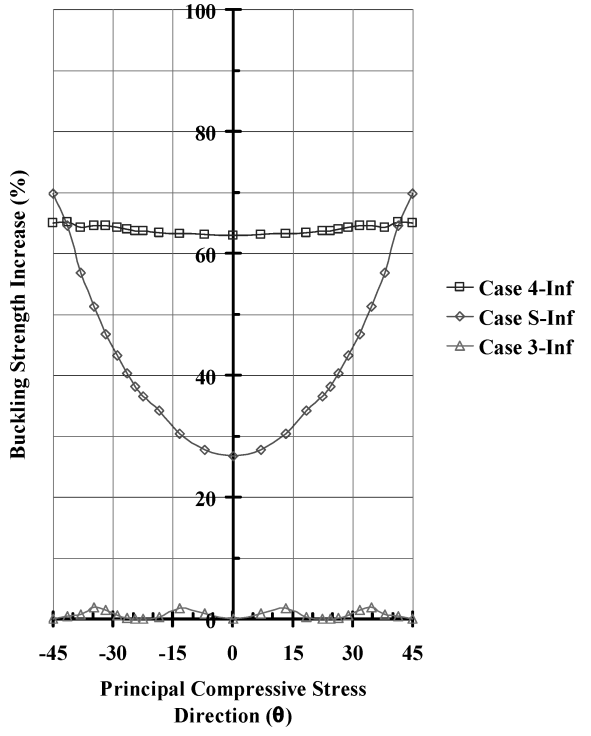

Fig. 2 Buckling-strength-increase comparisons, above the infinitely long datum (Case 1—Inf) with simply supported edges, for the three variants illustrated in Fig. 3.

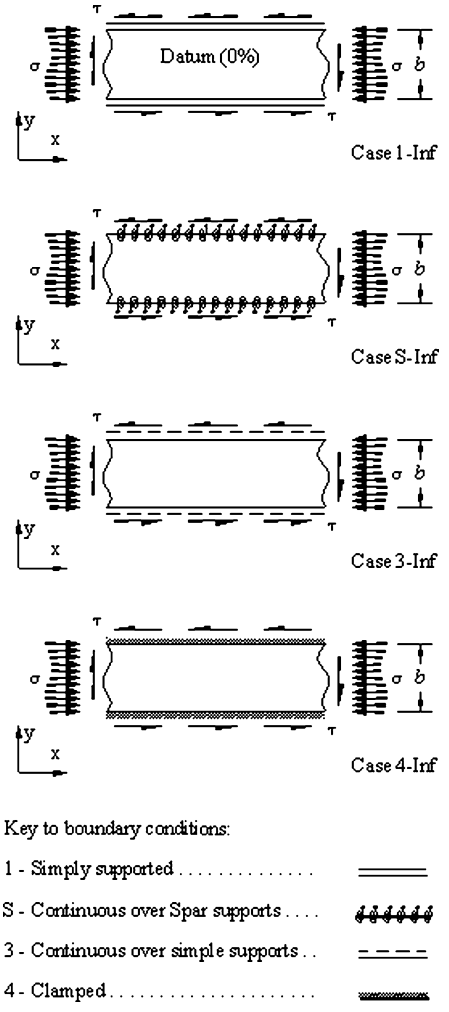

Fig. 3 Alternative boundary conditions for the infinitely long panel assumption.

Figure 4 shows the rectangular planform geometry and boundary conditions of the results illustrated in Fig. 5. Although there is no difference in the compression buckling strength ($\theta = 0$ deg) between the results of Figs. 2 and 5, the shear loaded cases show a marked increase due to the added constraint of the transverse supports.

Figure 6 shows the skew planform geometry and boundary conditions of the results illustrated in Fig. 7. These results illustrate strength increases above the infinitely long cases for the same reasons as the rectangular cases. The effect of skew planform is to increase the buckling strength of panels above the rectangular panel equivalent when compression, positive shear, or a combination of the two are predominant.

It should be noted that the spar-supported variants on Figs. 2, 5, and 7 have a higher-percentage strength increase than the clamped result for pure shear loading, $\theta = 45$ and -45 deg. This is because the rigid spar attachment reduces the effective width of the panel, leading to a higher buckling strength than the wider, datum panel. The width of the rigid attachment was assumed to be 10 mm (0.39 in.).

Figure 8 illustrates the final comparison of the preliminary-analysis series, applied to the skew bay planform. Here an increased panel thickness, incorporating 68 plies, is used together with a stiffener with 28 plies. These increases are consistent with the initial sizing results of finite element method (FEM) model of the entire aircraft. All other parameters are comparable with the previous data set. Because the panel thickness has now been increased substantially, a second set of results is presented, which takes account of TTS deformation effects.[4]

In all cases, the reduction in buckling strength caused by TTS effects, illustrated in Fig. 8, is relatively uniform across the load spectrum.

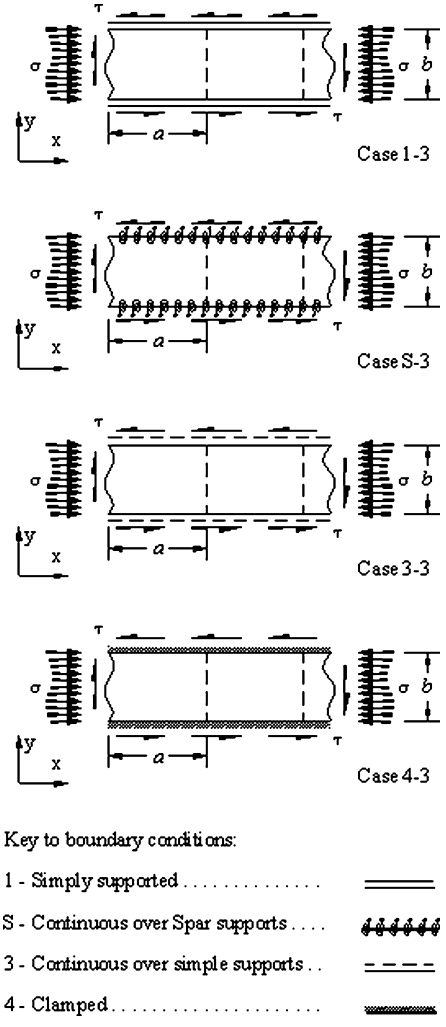

Fig. 4 Alternative boundary conditions for the rectangular bay assumption.

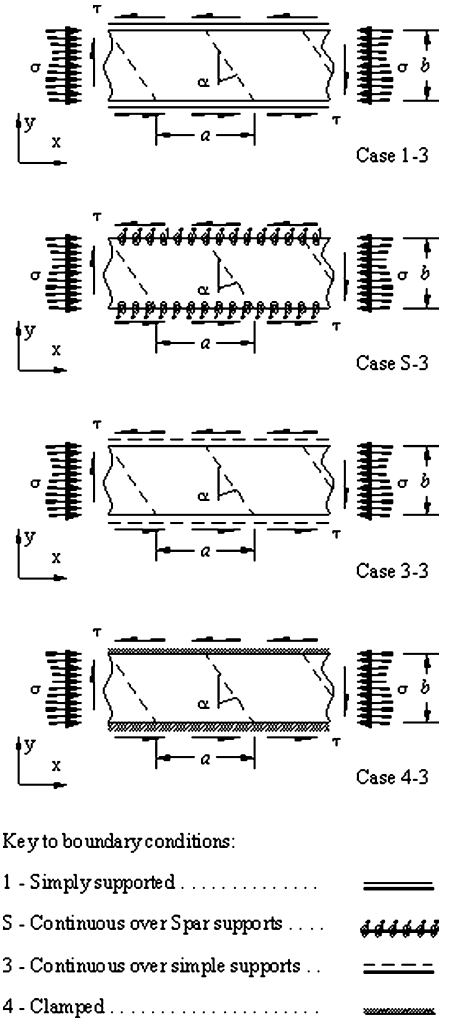

Fig. 6 Alternative boundary conditions for the skew bay assumption.

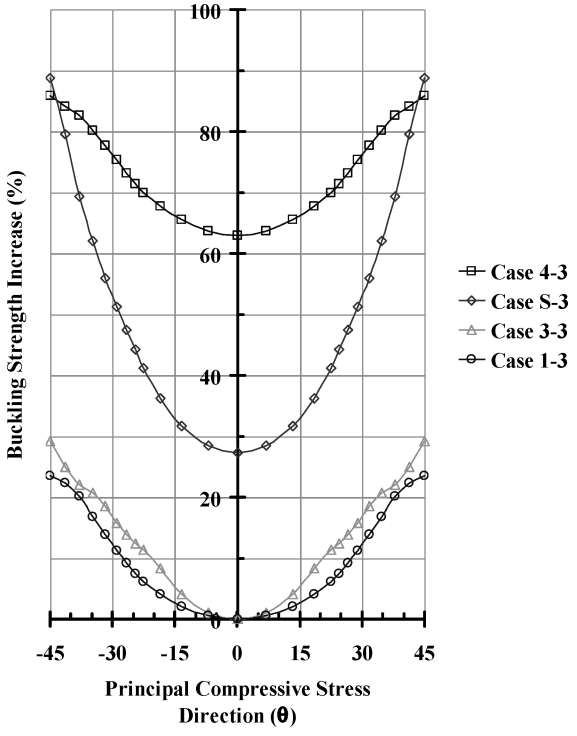

Fig. 5 Buckling strength increases above datum (Case 1—Inf) for panels continuous over rectangular bays ($a/b \approx 2.5$).

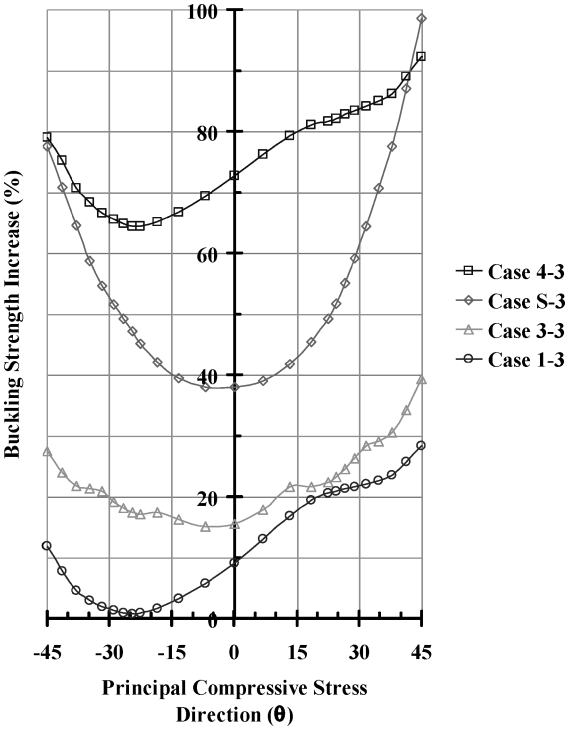

Fig. 7 Buckling strength increases above datum (Case 1—Inf) for panels continuous over skew bays ($a/b \approx 2.5$).

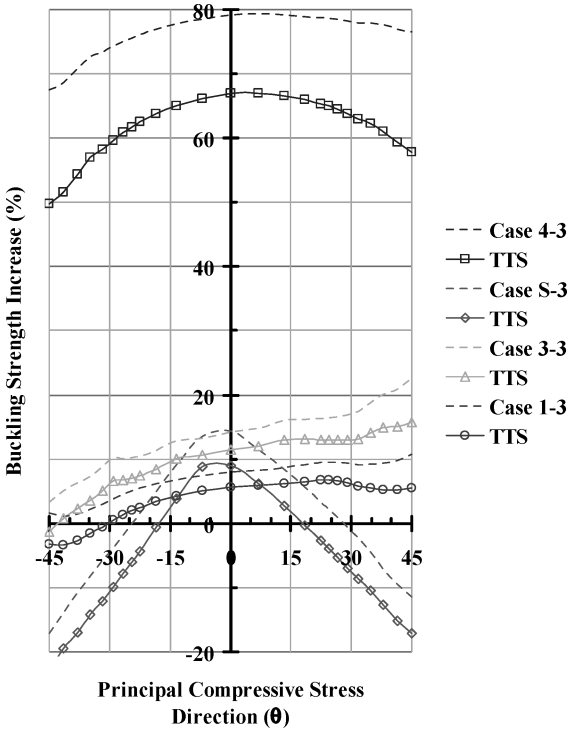

Fig. 8 Buckling strength increases above the modified datum (Case 1—Inf) for panels continuous over skew bays ($a/b \approx 3.0$), including through thickness shear (TTS) effects.

The results of Fig. 8 illustrate a marked difference in the behavior of the spar-supported variant, case S—3, as the consequence of an increased panel-skin/supporting-spar thickness ratio. A drastic strength reduction, below the datum (case 1—Inf), occurs across much of the loading range, except where compression load is dominant. By contrast, the boundary conditions of case 1—3, case 3—3, and case 4—3 provide rigid out-of-plane constraint, and therefore the magnitude of the buckling strength increases, above the datum (case 1—Inf), is comparable with the previous results.

This final set of results indicate that the flexibility of the (unloaded) supporting spar is such that the mode shape of the buckled skin panel is inconsistent with the spar pitch and implies that the spar thickness is adequate.

In a real wing box, the spars transfer shear and bending stresses between the compression-loaded top skins and tension-loaded bottom skins. These characteristics have not been captured by the modeling used thus far. Hence, a more sophisticated model is now considered, in which the full channel section spar is incorporated together with the associated portion of the top and bottom skins (see Fig. 9b). A bending moment is applied to the section together with in-plane shear and transverse compressive skin loads. This loading combination is then consistent with results obtained from average element stresses taken from a static FEM analysis of the entire aircraft (see Table 1).

This new and more complex model demonstrated buckling strengths consistent with the spar-supported cases of Figs. 2, 5, and 7 of the preliminary-analysis section and is the model adopted for the optimum-design study that follows.

III. Optimum-Design Study

A. Details of the Modeling Used

The previous section of this paper explored various levels of modeling sophistication to show the effects of analyzing the panel with its true skewed shape rather than approximating it as rectangular in plan and the level to which modeling approximations may be safely applied, for example, unloaded spar supports.

In the next section of the paper, attention is focused on the minimum-mass design of multispar wing-box panel structures and

Table 1 Applied moments (in-lbs) and in-plane compressive loading and shear flow (lbs/in)

Loading	Case 1	Case 2	Case 3	Case 4
M_y	−488,814	−24,289	−452,468	−59,613
(N_x)	(11,350)	(564)	(10,506)	(1,384)
N_y	1,146	115	985	208
N_{xy}	−2204	−107	−1,683	−605

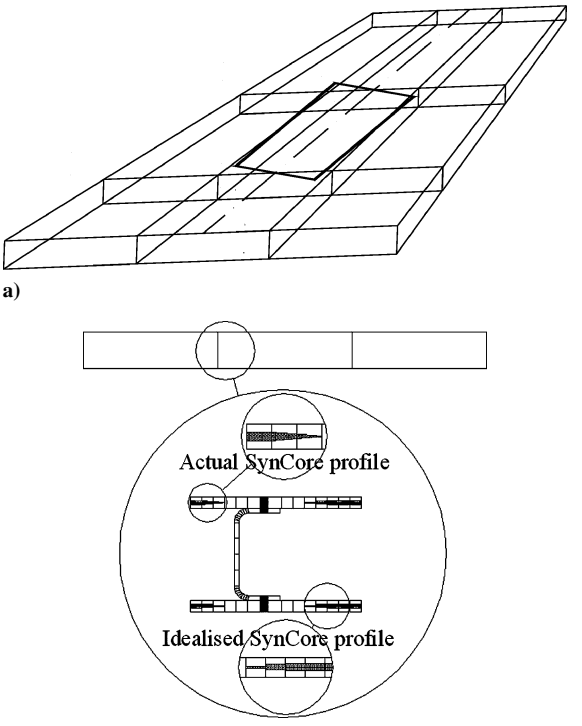

Fig. 9 Parts: a) sketch of empennage wing structure illustrating the rectangular panel idealization with length $a = 49.667$ in. and width $b = 16.556$ in. b) detail of the prismatic wing-box idealization for the computer model incorporating a repeating spar with associated top and bottom panel skin, the width of which depends on the number (variable) of spars in the wing box. Also shown is the SynCore idealization, with discrete step thickness increase, compared with the actual smooth-taper profile.

the effects of incorporating a lightweight syntactic (meaning filled with high-strength hollow glass spheres) film core (SynCore™) as a partial replacement for carbon-fiber composite material.

A rectangular panel approximation is used throughout the optimization study, for which the geometry was obtained by first calculating the length between ribs, measured along the centerline of the panel on Fig. 9a, to obtain the length $a(=49.667$ in.). The width $b(=16.556$ in.) of each panel was derived from its mid-length width, which was then transformed to account for the sweep of the wing.

Figure 9b gives details of the wing-box idealization, which is used throughout the optimization study. Here the computer model forms a prismatic, open section, transversely repetitive "single-cell" representation of the wing box, which incorporates a common repeating-channel section spar with associated top and bottom panel skin, the width of which depends on the number (variable) of spars in the wing box.

The initial geometry, or "start" design, was established for the panel variants by using the minimum-gauge ply thickness of 0.1397 mm (0.0055 in.) for each laminate of the panel assembly and setting the panel breadth to that of the three-bay, four-spar configuration illustrated in Fig. 9a, which has an aspect ratio $a/b = 3.0$.

The use of SynCore as partial replacement of carbon-fiber material is now introduced. The SynCore is placed at the neutral axis of a laminated composite wing skin and of constant thickness, $t_{\text{SynCore}} = 0.121$ in., equivalent to 22 carbon-fiber plies. A density

comparison reveals that SynCore (0.0252 lb/in.^{3}) is less than half that of carbon-fiber material (0.057 lb/in^3). Figure 9b illustrates the SynCore material, which is introduced into the laminate using a tapered profile, over a distance of approximately 0.6 in., that is, a 1:5 gradient with an edge distance of approximately 0.715 in. from the spar. Note that for practical considerations, SynCore material must be discontinued in the region of the skin/spar attachment. However, from a buckling perspective, the strength of the panel would be reduced by 2.9%, based on load case 1 of Table 1, if SynCore was continuous across the spar cap.

For computational expedience, all optimum-design results were obtained using the VIPASA coding,[8] which is retained as a VICONOPT option. This and other simpler analysis methods, which are frequently used for design, do not couple wavelengths of the buckling response[9,10] and thus may give relatively conservative results, hence higher mass solutions. This tendency was shown by an extensive study[11] to be typical of panels that have significant shear-load (N_{xy}) contributions and are governed by overall buckling.

In keeping with the philosophy of the GARTEUR work, described in the introductory section, the results presented in this new study all used the same number of wavelengths, $\lambda = a/i$ ($i = 1, 2, 3, \ldots, 10$). Therefore, even though the results may have an element of approximation, any errors should be of the same magnitude for all of the problems and conclusions about the percentage mass savings obtained by the various refinements considered should remain valid.

Laminate stacking sequences giving special orthotropic properties are adopted so that the exact closed-form solution may be used to calculate the buckling strength without the need for complex numerical calculations or as a check for errors. This choice also maximizes the buckling strength in comparison to a general balanced and symmetric-angle ply laminate possessing anisotropic bending stiffness properties, that is, bend–twist coupling.

An important consideration when designing the ply-stacking sequence is that it has consistent behavior when SynCore is used as a partial replacement, implying that the in-plane and out-of-plane behavior remains uncoupled ($B_{ij} = 0$) and additionally, in this case, that the special orthotropic nature of the material is maintained ($A_{16} = A_{26} = D_{16} = D_{26} = 0$). This was achieved through the addition of symmetric and antisymmetric stacking sequences, which together maintain this special orthotropic nature when SynCore film is introduced along the mid-plane of the laminate.

The buckling design results that follow provide a comparison of optimum mass configurations for variants of the panel shown in Fig. 9b when required to carry all four of the load cases of Table 1. These panel loads were derived from a FEM model of the complete aircraft. The variation in axial stress (tension to compression) between top and bottom skin is accounted for by means of a bending moment applied to the wing-box model. The bending moment was calculated from the aerodynamic loading on the wing and verified against the average element stresses of the FEM model. In contrast, shear flow is assumed to be constant across individual skins and spars and was checked against both average element stresses of the FEM model and a hand solution for the determination of skin shear flows in a multicell wing box.[12,13] Note that although an increase in the number of spars will reduce the shear load in these components, this is not accounted for in the optimum-design process undertaken in this study.

The material properties used in the study are given in Table 2. These include the strain-constraint data that need only be applied to the carbon-fiber material because of the large difference in modulus.

The majority of results presented are for panel skins consisting of a 62-ply laminate, $[A1/S1/0/90/A83/90/0/S1/A1]_T$, in which ply groupings A1, S1, and A83, using engineering sciences data unit (ESDU) shorthand notation,[14] signify the stacking sequences $[\pm 45/-45/45]_A$, $[45/-45_2/0/45/0]_S$, and $[45/90/-45_2/0/45/0/90/0]_A$, respectively. The stacking sequence of the invariant 28-ply laminate spar is $[\pm 45/0/-45/90_2/45_2/90_2/-45/0/-45/45]_S$. The start design thickness of the skin (0.341 in.) is therefore approximately twice that of the supporting spar (0.154 in.).

Subscripts A, S, and T imply the sequence given in brackets is the top antisymmetrical half, the top symmetrical half, and the true (or total) listing of the stacking sequence forming the laminate.

One variant on the skin-ply-stacking sequence, used later to overcome strain-constraint requirements arising from SynCore fiber replacement, adopts a 70-ply laminate with similar ply groupings: $[S1/S1/0/90/A83/90/0/S1/S1]_T$.

Computer modeling accounts for continuity of the skin over composite curved-root channel-section spars, assumed to be connected by a single line of bolts, which are accounted for in the weight assessment (see Table 3). The outer mold line of the wing box is maintained by linking spar depth (dependant variable) and skin-ply thicknesses (independent variable). It should be noted, however, that an optimum design with a ply thickness other than the start design thickness ($t = 0.0055$ in.) implies that the stacking sequence must be redesigned.

B. Optimum Design Results

The optimum mass results, given in the tables that follow, are presented across a series of 11 columns. The first column of each table indicates the unique case number to which each variant is

Table 3 Fastener details accounted for in the weight assessment

Parameter	Value
Mass per metal fastener	0.0329 lbs
Mass of carbon fiber material removed per fastener	0.0014 lbs
Fastener spacing	1.5 in.

Table 2 Material properties for carbon/epoxy composite[15] and lightweight SynCore

		Carbon/epoxy IM7/8552		SynCore HC 9872	
Material properties	Symbol	Metric units	Imperial units	Metric units	Imperial units
Compressive moduli	E_1	143 GPa	20,740,397 psi	2.6 GPa	375,000 psi
	E_2	9.6 GPa	1,392,362 psi	2.6 GPa	375,000 psi
Shear modulus ($G_{13} = G_{23} =$)	G_{12}	5.2 GPa	754,196 psi	1.0 GPa	150,000 psi
Poisson's ratio	ν_{12}	0.338	0.33		
Density	ρ	1.57 g/cm^3	0.057 lb/in^3	0.69 g/cm^3	0.025 lb/in^3
Tensile moduli	E_1	176 GPa	25,526,643 psi	2.8 GPa	400,000 psi
	E_2	8.9 GPa	1,290,836 psi	2.8 GPa	400,000 psi
Compressive strength	σ_1	885 MPa	128,358 psi	60.7 MPa	8,800 psi
	σ_2	233 MPa	33,794 psi		
	τ_{12}	56.3 MPa	8,166 psi	41.4 MPa	6,800 psi
Tensile strength	σ_1	2,352 MPa	341,128,774 psi	33.1 MPa	4,800 psi
	σ_2	47 MPa	6,816,774 psi		
Strain allowable (comp.)	ε_1	0.006188			
	ε_2	0.024270			
	γ_{12}	0.010826			
Strain allowable (tension)	ε_1	0.013363			
	ε_2	0.052800			

Table 4 Laminate (62-ply): ply thickness variable (start design: $t = 0.0055$ in.). Note that column (2) also represents the aspect ratio (a/b) of the panel

(1) Case	(2) No. bays	(3) No. spars	(4) Spar pitch	(5) t_{opt}	(6) M_{Popt}	(7) M_{Popt}/M_{P0}, %	(8) M_{Wopt}	(9) M_{Wopt}/M_{W0}, %	(10) M_{Topt}	(11) M_{Topt}/M_{T0}, %
1	1	2	49.7	0.00536	95.8	179.3	97.9	−6.8	100.0	−8.4
2	2	3	24.8	0.00364	34.2	−0.4	70.5	−32.8	73.7	−32.5
3	3	4	16.6	0.00308	20.3	−40.7	63.3	−39.8	67.5	−38.2
4	4	5	12.4	0.00266	14.1	−59.0	58.6	−44.2	63.9	−41.5
5	5	6	9.9	0.00228	10.4	−69.6	54.5	−48.1	60.9	−44.2
6	6	7	8.3	0.00235	9.3	−72.7	58.4	−44.4	65.8	−39.7

Table 5 Laminate (62-ply) with strain constraints: ply-thickness variable (start design: $t = 0.0055$ in.)

(1) Case	(2) No. bays	(3) No. spars	(4) Spar pitch	(5) t_{opt}	(6) M_{Popt}	(7) M_{Popt}/M_{P0}, %	(8) M_{Wopt}	(9) M_{Wopt}/M_{W0}, %	(10) M_{Topt}	(11) M_{Topt}/M_{T0}, %
13[a]	1	2	49.7	0.00536	95.8	179.3	97.9	−6.8	100.0	−8.4
14	2	3	24.8	0.00462	42.6	24.3	87.4	−16.7	90.6	−17.0
15	3	4	16.6	0.00461	29.2	−14.9	89.7	−14.6	93.9	−14.0
16	4	5	12.4	0.00462	22.5	−34.5	92	−12.4	97.2	−10.9
17	5	6	9.9	0.00462	18.5	−46.2	94.4	−10.1	100.7	−7.8
18	6	7	8.3	0.00460	15.8	−54.1	96.7	−7.9	104	−4.7

[a]Strain constraints not active.

Table 6 Laminate (62-ply) with SynCore replacement: ply-thickness variable (start design: $t = 0.0055$ in.)

(1) Case	(2) No. bays	(3) No. spars	(4) Spar pitch	(5) t_{opt}	(6) M_{Popt}	(7) M_{Popt}/M_{P0}, %	(8) M_{Wopt}	(9) M_{Wopt}/M_{W0}, %	(10) M_{Topt}	(11) M_{Topt}/M_{T0}, %
7	1	2	49.7	0.00717	100.8	193.9	102.9	−2.1	104.9	−3.9
8	2	3	24.8	0.00369	31.5	−8.2	65.2	−37.9	68.4	−37.4
9	3	4	16.6	0.00260	17.4	−49.4	54.3	−48.3	58.6	−46.4
10	4	5	12.4	0.00205	11.8	−65.5	49.6	−52.8	54.9	−49.7
11	5	6	9.9	0.00197	9.7	−71.8	50.7	−51.7	57.1	−47.7
12	6	7	8.3	0.00218	9.0	−73.9	56.1	−46.6	63.5	−41.9

Table 7 Laminate (62-ply) with SynCore replacement and strain constraints: ply-thickness variable (start design: $t = 0.0055$ in.)

(1) Case	(2) No. bays	(3) No. spars	(4) Spar pitch	(5) t_{opt}	(6) M_{Popt}	(7) M_{Popt}/M_{P0}, %	(8) M_{Wopt}	(9) M_{Wopt}/M_{W0}, %	(10) M_{Topt}	(11) M_{Topt}/M_{T0}, %
19	1	2	49.7	0.00987	132.7	286.7	134.5	28.1	136.6	25.1
20	2	3	24.8	0.00865	62.1	81.0	126.1	20.1	129.2	18.3
21	3	4	16.6	0.00775	39.5	15.2	120.5	14.8	124.7	14.2
22	4	5	12.4	0.00705	28.6	−16.5	116.6	11.0	121.8	11.5
23	5	6	9.9	0.00648	22.3	−34.9	113.7	8.3	119.9	9.8
24	6	7	8.3	0.00599	18.2	−46.9	111.3	6.0	118.6	8.6

Table 8 Laminate (62-ply) with variable skin breadth, with constant ply thickness, and using 1-bay, 2-spar configuration as start design, i.e., spar pitch = 49.7 in. Cases 25–28 represent the carbon-fiber laminate, the laminate with strain constraints, the SynCore variant, and the SynCore variant with strain constraints, respectively

(1) Case	(2) No. bays	(3) No. spars	(4) Spar pitch	(5) t_{opt}	(6) M_{Popt}	(7) M_{Popt}/M_{P0}, %	(8) M_{Wopt}	(9) M_{Wopt}/M_{W0}, %	(10) M_{Topt}	(11) M_{Topt}/M_{T0}, %
25	$a/b = 5.61$	8.8	0.0055	19.4	−43.4	111.1	5.8	118.0	8.1	
26	$a/b = 1.65$	30.2	0.0055	60.6	76.7	101.9	−3.0	104.6	−4.2	
27	$a/b = 1.76$	28.2	0.0055	47.8	39.4	86.4	−17.7	89.3	−18.2	
28[a]	$a/b = 0.97$	51.0	0.0055	83.1	142.3	83.1	−20.9	85.2	−22.0	

[a]Strain constraints not satisfied.

henceforth referred. Columns 2 and 3 indicate the number of bays and spars, respectively. By coincidence, column 2 also corresponds to the aspect ratio (a/b) of the panel (see Fig. 9). Column 4 is the spar pitch, obtained from the wing-box width (=49.667 in.) divided by the number of bays (column 2).

Column 5 gives the optimized ply thickness t_{opt}. Note that in Tables 4–8 there are 62 plies in the laminate skin, giving a total laminate thickness of 0.341 in., using the start design ply thickness of 0.0055 in.

Columns 6 and 7 provide the optimized panel mass M_{Popt} and the change in mass M_{Popt}/M_{P0} (%), expressed as a percentage of the datum panel M_{P0}. The panel mass is derived from the model of Fig. 9b, which includes spar and associated top and bottom skins. The datum mass, corresponding to the three-bay, four-spar configuration of Fig. 9 is $M_{P0} = 34.3$ lbs and is used for all the comparisons that follow. A negative M_{Popt}/M_{P0} (%) value in column 7 indicates a mass reduction, whereas a positive value indicates an increased mass design.

Columns 8 and 9 provide the optimized wing-box mass M_{Wopt} and the change in mass M_{Wopt}/M_{W0} (%), expressed as a percentage of the datum panel, $M_{W0} = 105$ lbs.

Column 10 provides the total optimized wing-box mass, which includes fasteners M_{Topt} (see Table 3). Finally, column 11 gives the change in mass M_{Topt}/M_{T0} (%), expressed as a percentage of the datum panel $M_{T0} = 109.2$ lbs.

The tabulated results are grouped according to the particular variable being investigated. Each table contains six aspect-ratio configurations for which the optimum ply thickness is determined.

Table 9 Laminate (62-ply) with variable skin breadth and ply thickness, using 1-bay, 2-spar configuration as start design, i.e., spar pitch = 49.7 in., and with SynCore replacement and strain constraints

(1) Case	(2) No. bays	(3) No. spars	(4) Spar pitch	(5) t_{opt}	(6) M_{Popt}	(7) M_{Popt}/M_{P0}, %	(8) M_{Wopt}	(9) M_{Wopt}/M_{W0}, %	(10) M_{Topt}	(11) M_{Topt}/M_{T0}, %
28a	$a/b = 0.81$		61.4	0.0075	127.2	270.8	104.9	0.1	106.8	−2.2

Table 10 Laminate (70-ply) (including 22-ply equivalent SynCore material) with variable skin breadth and ply thickness and using 1-bay, 2-spar configuration as start design, i.e., spar pitch = 49.7 in.

(1) Case	(2) No. bays	(3) No. spars	(4) Spar pitch	(5) t_{opt}	(6) M_{Popt}	(7) M_{Popt}/M_{P0}, %	(8) M_{Wopt}	(9) M_{Wopt}/M_{W0}, %	(10) M_{Topt}	(11) M_{Topt}/M_{T0}, %
29	$a/b = 1.14$		43.6	0.0060	88.1	156.9	102.5	−2.4	104.7	−4.1

Tables 4 and 5 correspond, respectively, to the 62-ply carbon-fiber material and the 62-ply carbon-fiber material including strain constraints.

Results in Table 6 correspond to panels with partial replacement of carbon-fiber plies using lightweight syntactic film core (SynCore) material. The SynCore has a constant thickness, equivalent to 22 carbon plies, and is placed at the laminate mid-plane (see Fig. 9b). Hence, only 40 of the 62 (variable-thickness) carbon plies remain. Table 7 presents the same laminate configuration results as Table 6, but material-strain constraints are now included in the optimum-design process.

Some specific observations on the optimum results of Table 4 to Table 7 now follow:

In Table 4, the optimum case 1 ply thickness ($t_{opt} = 0.00536$ in.) is virtually unchanged from the start design thickness ($t = 0.0055$ in.), indicating that the width of the bay is near optimum for the given stacking sequence. Note that the ply thickness must correspond to the actual ply thickness of 0.0055 in. Any variation in ply thickness indicates that the stacking sequence must be redesigned with a different number of plies of thickness 0.0055 in. The remaining results of Table 4 indicate that the optimum design (case 5) for the carbon-fiber laminate skin configuration is to increase the number of bays, or spars, in the wing box, which leads to skins (0.141 in.) and spars (0.154 in.) of similar thickness.

The case 7 result of Table 6, corresponding to the one-bay, two-spar configuration with SynCore replacement, reveals an optimum ply thickness that appears to be considerably higher than case 1, that is, $t_{opt} = 0.007171$ compared with 0.004644. In this case, however, the SynCore is of constant thickness; hence, the total skin thickness (0.408 in.) is only marginally higher than the carbon skin (0.332 in.) of case 1.

As expected, the other results of Table 6 follow a similar trend to those of Table 4, with the SynCore variant resulting in a mass savings of approximately 5%, because the use of lightweight material at the laminate mid-plane has a marginal effect on the bending stiffness, hence the buckling strength.

Comparison of Tables 5 and 7 demonstrates the severe effect that in-plane strain constraints have on the minimum mass design when SynCore is used as a partial replacement for carbon fiber material. In this case, the use of SynCore as a partial replacement has failed to achieve a mass savings over the full carbon-fiber-laminate datum panel. For example, in case 19, the variable carbon-fiber ply thickness has increased from the start design of 0.0055 in. to 0.009868 in. to compensate for the reduced in-plane stiffness of the SynCore material. By contrast the strain limits for the full carbon-fiber laminate of case 13 are not reached. Comparison of the ply thickness t_{opt} in Tables 6 and 7 implies that in meeting the strain constraint the panels now have a significant buckling-strength margin. Therefore, for economical design the panel width must be increased until the buckling constraint is active.

Table 8 presents a set of results for which the ply thickness is held constant and instead the spar pitch is used as the design variable. This is a more realistic design process, given that the laminate has a predefined stacking sequence with realistic ply thickness. However, it was not used in the main study because skew panels were a design consideration (although they are not presented in the current paper), which requires a constant panel width to maintain the correct skew angle of the line of point supports.

Case 25 has failed to produce a mass savings over the datum case, converging on a configuration similar to the optimum (case 5) of Table 4 but with thicker skin. The case 26 result (carbon-fiber laminate with variable bay width and material-strain constraints) has converged on the most critical strain constraint, with a buckling reserve factor of 11%. The case 27, SynCore variant, result has converged on 1.76 bay-width equivalents. However, the result for case 28, which corresponds to the SynCore variant with strain constraints, has failed to satisfy the strain constraints. This result implies that direct replacement of SynCore, on a ply-by-ply basis, will generally be unable to satisfy the strain constraints. To investigate this further, the ply thickness of the carbon plies in case 28a are allowed to vary, along with the panel width. The results are demonstrated in Table 9.

The spar pitch has increased to reduce the buckling reserve factor of the thicker laminate (equivalent to 74 plies) required to satisfy the strain constraints. However, this carbon-ply thickness t_{opt} is no longer representative of the real ply thickness. Therefore, as a further test, a modified 70-ply special orthotropic laminate is adopted, using the same SynCore thickness as before, that is, equivalent to 22 carbon plies. The details of this laminate are given in Table 2 and the results are presented in Table 10.

These results demonstrate that ply thickness for the 70-ply laminate is close to optimum; hence, the value of t_{opt} (=0.0060) is virtually unchanged from the start design ($t = 0.0055$).

The results of case 26 (62-ply carbon-fiber laminate) and case 29 (48-ply carbon-fiber laminate with 22-ply equivalent SynCore material) offer a comparison of the beneficial use of SynCore as a partial replacement for carbon-fiber material, where both buckling and strain constraints are satisfied. Although neither result offers a spar pitch exactly compatible with the overall wing-box dimension (49.7 in.), it can be seen that the spar pitch of case 29 SynCore variant (43.6 in.) is close enough to estimate that the mass savings will not change significantly from 4.1%. By contrast, the optimum design of full carbon-fiber laminate, giving a 4.2% mass savings, is likely to be reduced substantially when the panel width is necessarily adjusted.

IV. Conclusions

Minimum mass-buckling design results have been presented for multispar composite wing-box structures based on the infinitely long plate assumption. Although these results are not expected to differ greatly for a rectangular plate with an aspect ratio $2.5 \le a/b \le 3.0$, they are likely to be highly conservative (upper bound) if they are used to approximate panels with a skewed platform.

The results have demonstrated the potential mass savings of incorporating a lightweight syntactic-film core (SynCore) as a partial replacement for carbon-fiber plies, considering buckling-strength and limiting strain constraints. The buckling strength is not significantly degraded by this partial replacement, because the bending stiffness of the panel is not substantially affected by the removal of high-strength material at the laminate mid-plane. However, the relative in-plane stiffness of SynCore (400,000 lb/in.^{2}), being much lower than the carbon fiber (22,180,000 lb/in.^{2}) it replaces, leads to a substantial reduction in the margin of the material-strain constraint.

The results have demonstrated that the use of SynCore, as an economic partial replacement for carbon-fiber material, leads away from the multicell or multispar design configuration, toward a single-cell configuration in which the skin thickness required to satisfy the strain constraints can be matched by a panel width that just satisfies the buckling constraint.

Results based on the infinitely long plate assumption have shown that a lower mass solution cannot be obtained by the use of SynCore as a partial (≈35%) replacement of carbon-fiber plies, on a ply-by-ply basis where the strain constraints are found to be active. In this case, it was necessary to augment the laminate thickness by additional carbon-fiber plies (≈8%), leading to a relative reduction in the SynCore content (≈30%).

Acknowledgments

The author gratefully acknowledges David Kennedy for facilitating the use of the VICONOPT computer code at Cardiff University, which was used to generate the new optimum-design results reported in this paper, and BAE Systems and the Royal Academy of Engineering for their financial support during the industrial secondment from which this work flows.

References

[1]York, C. B., Williams, F. W., Kennedy, D., and Butler, R., "A Parametric Study of Optimum Designs for Benchmark Stiffened Wing Panels," *Composites Engineering*, Vol. 3, Nos. 7–8, 1993, pp. 619–632.

[2]Williams, F. W., Anderson, M. S., Kennedy, D., Butler, R., and Aston, G., "User Manual for VICONOPT: An Exact Analysis and Optimum Design Program Covering the Buckling and Vibration of Prismatic Assemblies of Flat In-Plane Loaded, Anisotropic Plates, with Approximations for Discrete Supports, and Transverse Stiffeners," NASA-CR-181966, April 1990.

[3]Butler, R., and Williams, F. W., "Optimum Design Using VICONOPT, a Buckling and Strength Constraint Program for Prismatic Assemblies of Anisotropic Plates," *Computers and Structures*, Vol. 43, No. 4, 1992, pp. 699–708.

[4]Anderson, M. S., and Kennedy, D., "Inclusion of Transverse Shear Deformation in Exact Buckling and Vibration Analysis of Composite Plate Assemblies," *Proceeding of the 33rd AIAA/ASME/ASCE/AHS/ASC Structures, Structural Dynamics and Materials Conference*, AIAA, Washington, DC, 1992, pp. 283–291.

[5]Williams, F. W., and Anderson, M. S., "Buckling and Vibration Analysis of Shear-Loaded Prismatic Plate Assemblies with Supporting Structures, Utilizing Symmetric or Repetitive Cross-Sections," *Aspects of the Analysis of Plate Structures—A Volume in Honour of W. H. Wittrick*, edited by D. J. Dawe, R. W. Horsington, A. G. Kamtekar, and G. H. Little, Oxford University Press, Oxford, 1985, pp. 51–71.

[6]York, C. B., and Williams, F. W., "Theory and Buckling Results for Infinitely Wide Stiffened Skew Plate Assemblies," *Composite Structures*, Vol. 28, No. 2, 1994, pp. 189–200.

[7]Vanderplaats, G. N., "CONMIN—A FORTRAN Program for Constrained Function Minimisation, User's manual," NASA TM X-62282, Aug. 1973.

[8]Wittrick, W. H., and Williams, F. W., "Buckling and Vibration of Anisotropic or Isotropic Plate Assemblies Under Combined Loadings," *International Journal of Mechanical Sciences*, Vol. 16, No. 4, 1974, pp. 209–239.

[9]Anderson, M. S., and Stroud, W. J., "General Panel Sizing Computer Code and Its Application to Composite Structural Panels," *AIAA Journal*, Vol. 17, No. 8, 1979, pp. 892–897.

[10]Viswanathan, A. V., Soong, T. C., and Miller, R. E., "Compressive Buckling Analysis and Design of Stiffened Flat Plates with Multilayered Composite Reinforcement," *Computers and Structures*, Vol. 3, No. 2, 1973, pp. 281–297.

[11]Stroud, W. J., Greene, W. H., and Anderson, M. S., "Buckling Loads of Stiffened Panels Subjected to Combined Longitudinal Compression and Shear: Results Obtained with PASCO, EAL and STAGS Computer Programs," NASA TP 2215, Jan. 1984.

[12]Benscoter, S. U., "Numerical Transformation Procedures for Shear Flow Calculations," *Journal of the Institute of Aeronautical Sciences*, Vol. 13, No. 8, Aug. 1946, pp. 438–53.

[13]Samson, D. R., "The Analysis of Shear Distribution for Multi-cell Beams in Flexure by Means of Successive Numerical Approximations," *Journal of the Royal Aeronautical Society*, Vol. 58, Feb. 1954, pp. 122–127.

[14]Engineering Sciences Data Unit, "Laminate Stacking Sequences for Special Orthotropy," ESDU 82013, London, Oct. 1982.

[15]Rikards, R., Abramovich, H., Green, T., Auzins, J., and Chate, A., "Identification of Elastic Properties of Composite Laminates," *Mechanics of Advanced Materials and Structures*, Vol. 10, No. 4, 2003, pp. 335–352.